Combined effects of pressure and ionic strength on protein-protein interactions: an empirical approach

Supporting Information

Brian Paul[†,‡], Eric M. Furst[†], Abraham M. Lenhoff[†], Norman J. Wagner[†], and Susana C. M. Teixeira[†,‡,*]

[†] *Center for Neutron Science, Department of Chemical and Biomolecular Engineering, University of Delaware, Newark, DE 19716, United States.* [‡] *NIST Center for Neutron Research, National Institute of Standards and Technology, Gaithersburg, MD 20899, United States.* [*]Email: susanat@udel.edu

Oligomeric distribution of protein structure at 15 mg/mL ovalbumin in the absence of ammonium sulfate (AS)

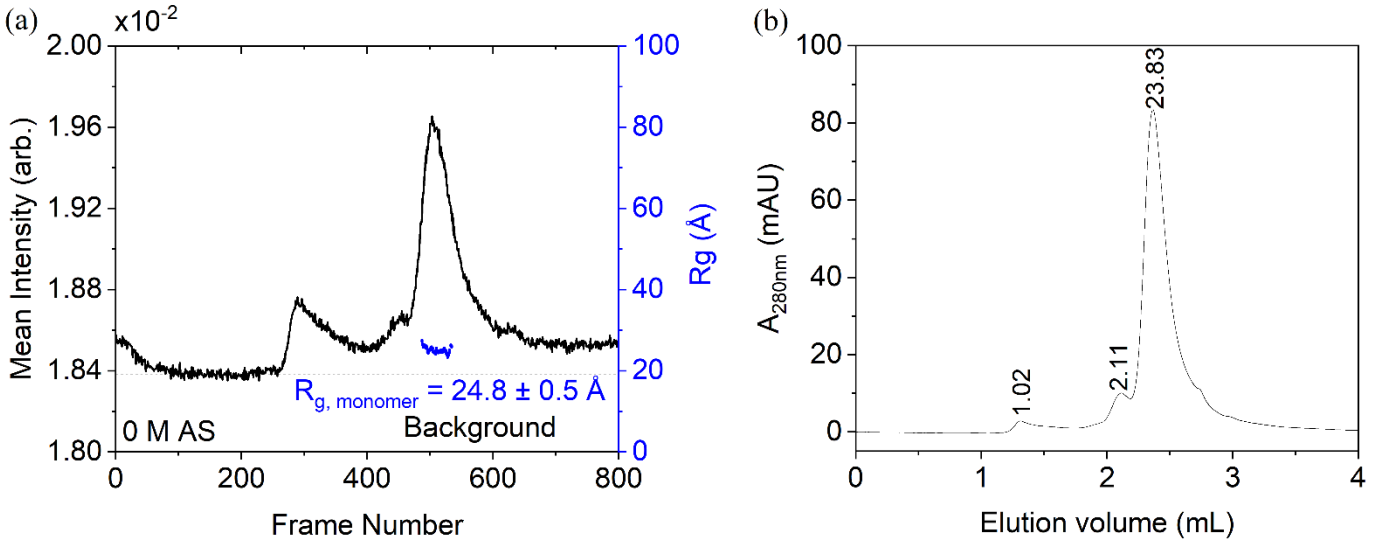

FIGURE S1. (a) X-ray scattered intensities for the SAXS-elution profile of AS-free ovalbumin solution in 5 mM phosphate buffer pD 7 (injection of 50 µL of protein solution at 15 mg/mL). The dashed line shows the background signal from buffer. The main peak radius of gyration R_g (blue) were calculated using liquid chromatography (LC) series analysis available in BioXTas RAW [1, 2]. The R_g of 24.8 Å fitted to the main peak is consistent with the monomer as the dominant species in solution. The average data for the main peak was used to produce a 1D scattering profile, which was then fitted to determine the reduced second virial coefficient b_2^*. **(b)** Corresponding UV absorption profile for the 4 mL elution measurement. The monomer peak (eluted at 2.5 mL) represents ≈88% of the total area of the absorbance intensity.

Dynamic light scattering

As shown in Figure S2, intensity autocorrelation function $g_2(Q, t_{lag})$ was measured using a DynaPro Nanostar II DLS instrument from Wyatt Corporation (Santa Barbara, CA), with a wavelength of 658 nm, as defined below:

$$g_2(Q, t_{lag}) = \frac{\langle I(Q,t) I(Q, t + t_{lag}) \rangle}{\langle |I(Q,t)|^2 \rangle} \quad \text{(S1)}$$

where $I(Q,t)$ and $I(Q, t + t_{lag})$ are the measured scattering intensities at a particular wave vector Q (which depends on the scattering angle and the refractive index of the medium), and times t and $t + t_{lag}$. t_{lag} is the time lag between intensity measurements [3]. Through the Siegert relation, $g_2(Q, t_{lag})$ can be converted to the field correlation function $g_1(Q, t_{lag})$:

$$g_2(Q, t_{lag}) = 1 + \beta \left| g_1(Q, t_{lag}) \right|^2 \quad (S2a)$$

where β is the intercept normalizing factor such that $[g_2(Q, t_{lag}) - 1]/\beta$ spans values between 0 and 1.

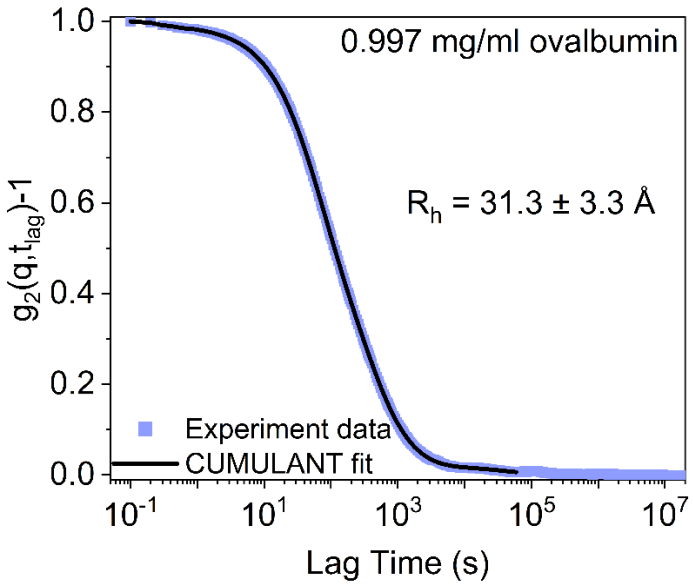

FIGURE S2: Cumulant fit to $g_2(q, t_{lag}) - 1$ for AS-free 0.997 mg/ml ovalbumin solution in 5 mM deuterated phosphate buffer (pD 7). The DLS data was collected at a scattering angle 90°, at 23°C. The average hydrodynamic radius was determined to be 31.3 Å, yielding $R_g/R_h \approx 0.776$, close to the expected average ratio of 0.775 for globular proteins [4].

From $g_1(Q, t_{lag})$, the CUMULANT analysis method was used to determine the decay rate Γ, which is related to the diffusivity D_0 and hydrodynamic radius R_h:

$$\Gamma = Q^2 D_0 \qquad (S3b)$$

$$R_h = \frac{k_B T}{6\pi\eta D_0} \qquad (S4c)$$

where Equation S2c is the Stokes-Einstein relation with η as the solvent viscosity, T as the solution temperature, and k_B as Boltzmann's constant.

Circular dichroism

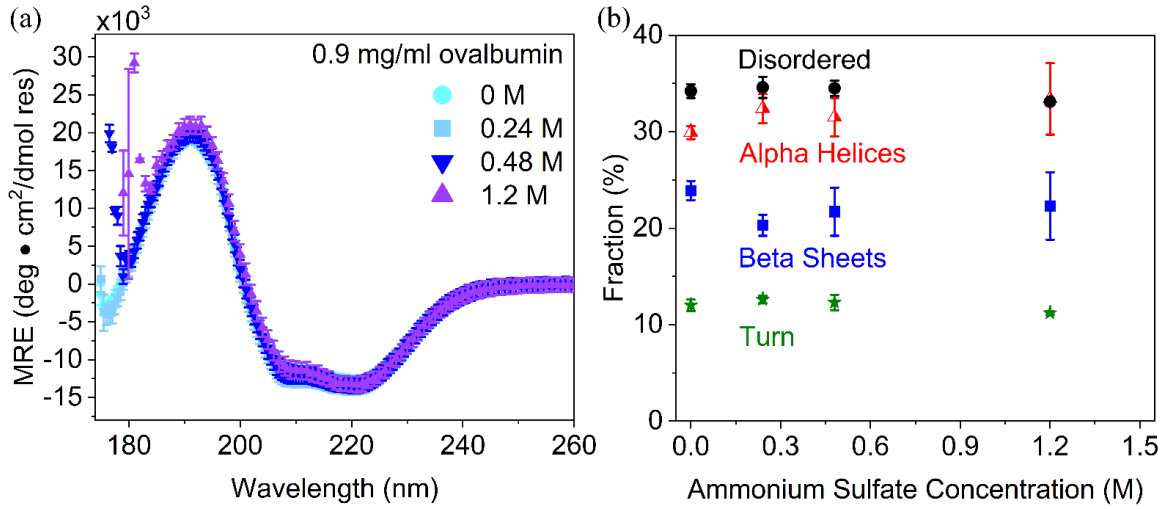

FIGURE S3. A: CD data shown as the mean residue ellipticity (MRE) for 0.9 mg/mL ovalbumin at room temperature with varying AS concentrations, color-coded as labeled. Error bars are standard errors in MRE based on three averaged measurements per condition. **B:** Secondary structure fractions determined from deconvolution of circular dichroism data using the CONTINLL algorithm in Dichroweb, and Reference data set SP175 [5-7]. The NRMSD for the fits to the 0, 0.24, 0.48, and 1.2 M AS solutions were 0.021, 0.024, 0.023, and 0.048, respectively. The error bars are standard errors between three successive deconvolutions at each condition.

The CD spectra in Figure S3 were obtained from Dichroweb [5] using the CONTINLL algorithm [7] to deconvolute the measured CD spectra as a function of different secondary structure contributions based on

the reference dataset SP175 [6]. The deviation between the experimental data and the reference set was quantified through the normalized root mean squared deviation (NRMSD) as defined below:

$$NRMSD = \sqrt{\frac{\sum_{\lambda}\left(\theta_{expt} - \theta_{calc}\right)^2}{\sum_{\lambda}(\theta_{calc})^2}} \qquad (S3)$$

θ_{expt} and θ_{calc} are the experimental and reference-calculated ellipticities at each wavelength λ, respectively. Smaller values measure the quality of the match between the experimental data and the reference data set. For the CONTILL method, an NRMSD ≤ 0.1 and a good match with the measured data is a good fit.

Ovalbumin solution structure: fits to SEC- SAXS data using a triaxial ellipsoid model

Table S1 shows the best-it parameters for SAXS data from an AS-free solution using a triaxial ellipsoid model (see equations 4 in the main document), as shown in Figure S4. The volume fraction and solvent SLD (coherent neutron scattering length density) were fixed as known parameters throughout the fits. The protein SLD was kept fixed to an initial value of 12 x 10^{-6} Å^{-1} for the first fits of the ellipsoidal radii.

Table S1: Triaxial ellipsoid fit parameters for SAXS data from an AS-free solution of 5 mg/ml ovalbumin.

Ra (Å)	Rb (Å)	Rc (Å)	Solvent SLD (10^{-6}/Å^{-2})	Protein SLD (10^{-6}/Å^2)	Volume fraction	χ^2
50.75 ± 0.17	21.32 ± 0.05	20.01 ± 0.04	9.35	12.19 ± 0.03	0.005	1.98

The parameter R_a is the polar radius, and R_b and R_c are the major and minor equatorial radii. χ^2 is a goodness-of-fit parameter and represents the minimized sum of weighted squares of the error (weighted residuals) between the data and the predicted fit [8].

Guinier Analyses and Form Factor Validation

The inset of Figure S4 shows the Guinier analysis of ambient pressure SAXS data measured for the 5 mg/mL ovalbumin solution (the fit parameters are shown in Table S2) used to obtain the radius of gyration R_g from an approximation of the low-Q data fitted with[9]:

$$ln\, I(q) = ln\, I(0) - \frac{R_g^2}{3} q^2 \qquad (S4)$$

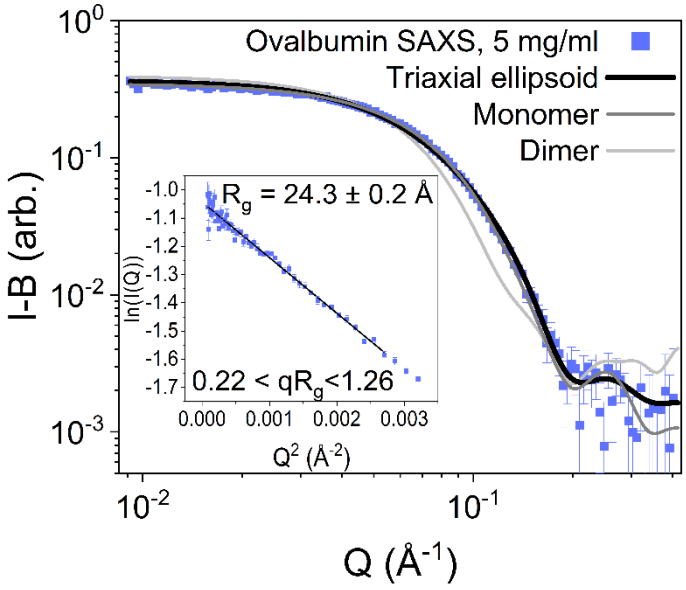

FIGURE S4. Ambient pressure SAXS data measured for 5 mg/mL ovalbumin solution in 5 mM sodium phosphate buffer pD 7 at room temperature. The buffer contributions have been subtracted from the data. The triaxial ellipsoid best-fit curve (black) is shown overlapping with the data (blue) and theoretical scattering calculated from the monomer (gray) and dimer (light gray) crystal structure [10]. Inset: Guinier fit to the low Q data, for radius of gyration determination, shown in black. Error bars arise from experimental counting statistics.

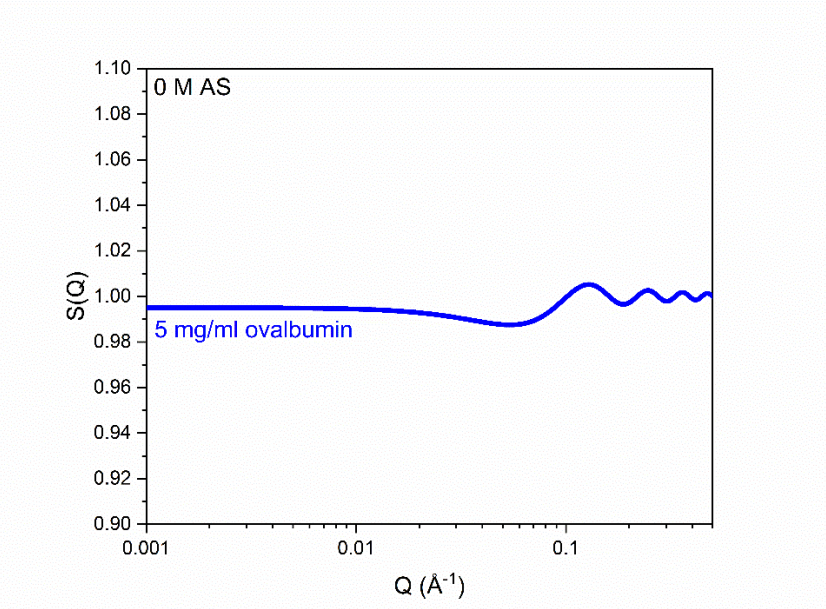

FIGURE S5. Structure factor profile calculated from b_2^* for AS-free 5 mg/ml ovalbumin, using the master curve equation to validate the initial assumption of no significant protein-protein interaction contributions to the corresponding SAXS data. The contribution from the structure factor to the scattering intensities are < 1% across the fit range (0.01 Å^{-1} < Q < 0.4 Å^{-1}).

Table S2. Best-fit parameters of Guinier analysis and distance distribution *P(r)* fits to ovalbumin scattering data in 5 mM deuterated phosphate buffer (in the absence of ammonium sulfate).

1 mg/ml ovalbumin	**Guinier Approximation Fit**			
	R_g (Å)	**I(0) (cm^{-1})**	**QR_g**	**R^2**
	24.7 ± 2.3	0.05 ± 0.001	0.27-1.26	0.92
	Inverse Fourier Transform Fit			
	R_g (Å)	**I(0) (cm^{-1})**	**D_{max} (Å)**	**Q_{min} - Q_{max} ($Å^{-1}$)**
	24.5 ± 3.5	0.05 ± 0.002	82.0	0.01-0.42
5 mg/ml ovalbumin	**Guinier Approximation Fit**			
	R_g (Å)	**I(0) (cm^{-1})**	**QR_g**	**R^2**
	24.3 ± 0.2	0.39 ± 0.002	0.21-1.29	0.98
	Inverse Fourier Transform Fit			
	R_g (Å)	**I(0) (cm^{-1})**	**D_{max} (Å)**	**Q_{min} - Q_{max} ($Å^{-1}$)**
	25.0 ± 0.2	0.39 ± 0.002	89.0	0.01-0.42
15 mg/ml ovalbumin	**Guinier Approximation Fit**			
	R_g (Å)	**I(0) (cm^{-1})**	**QR_g**	**R^2**
	24.8 ± 0.1	1.54 ± 0.004	0.29-1.29	0.98
	Inverse Fourier Transform Fit			
	R_g (Å)	**I(0) (cm^{-1})**	**D_{max} (Å)**	**Q_{min} - Q_{max} ($Å^{-1}$)**
	25.0 ± 0.1	1.54 ± 0.004	90.0	0.01-0.42

Fits were performed using the *BioXTas Raw* software package [2, 11]. R^2 is the goodness-of-fit for the linearized Guinier approximation.

Tabulated protein hard sphere radii and Baxter model parameters

Table S3. Hard sphere diameters for proteins studied, determined as twice the hydrodynamic radius as measured via dynamic light scattering (DLS), where $B_{22}^{HS} = 2\pi\sigma^3/3$.

Protein	$\boldsymbol{\sigma = D_{HS} = 2R_h}$ **(nm)**
Ovalbumin	6.3 ± 0.7
Lysozyme	3.8
β-lactoglobulin	7.0

The value for the hydrodynamic radius of ovalbumin was experimentally measured; values for lysozyme and β-lactoglobulin are taken from the literature [12, 13].

Table S4. Fitted stickiness values and calculated b_2^* for 15 mg/ml ovalbumin in 5 mM phosphate buffer, 23°C, pD 7 with varying ammonium sulfate concentration and applied hydrostatic pressure.

Ammonium Sulfate (M)	$P_{Applied}$ (MPa)	τ	b_2^*	Q Range (Å^{-1})	χ^2
0.00†	1	-	0.84 ± 0.15	0.008-0.34	-
0.20	1	0.97 ± 0.08	0.74 ± 0.10	0.008-0.34	1.53
0.50	1	0.36 ± 0.01	0.30 ± 0.05	0.008-0.34	2.91
0.80	1	0.21 ± 0.01	-0.18 ± 0.05	0.008-0.34	1.28
1.20	1	0.13 ± 0.01	-0.94 ± 0.02	0.008-0.34	1.64
1.36	1	0.10 ± 0.01	-1.40 ± 0.10	0.008-0.34	1.74
0.00†	10	-	0.83 ± 0.15	0.008-0.7	-
1.20	10	0.13 ± 0.01	-0.94 ± 0.04	0.008-0.7	8.66
1.36	10	0.10 ± 0.01	-1.46 ± 0.04	0.008-0.7	18.84
0.00†	98	-	0.57 ± 0.15	0.008-0.7	-
1.20	98	0.11 ± 0.01	-1.38 ± 0.07	0.008-0.7	6.68
1.36	98	0.07 ± 0.01	-2.37 ± 0.04	0.008-0.7	1.83
0.00†	195	-	0.35 ± 0.15	0.008-0.7	-
1.20	195	0.09 ± 0.01	-1.80 ± 0.09	0.008-0.7	5.04
1.36	195	0.06 ± 0.01	-3.18 ± 0.08	0.008-0.7	2.58
0.00†	265	-	0.12 ± 0.15	0.008-0.7	-
1.20	265	0.08 ± 0.01	-2.29 ± 0.06	0.008-0.7	5.58
1.36	265	0.06 ± 0.01	-3.34 ± 0.10	0.008-0.7	3.24
0.00†	350	-	-0.46 ± 0.15	0.008-0.7	-
1.20	350	0.07 ± 0.01	-2.74 ± 0.06	0.008-0.7	6.49
1.36	350	0.06 ± 0.01	-3.35 ± 0.10	0.008-0.7	3.13

†The reduced second virial coefficients for 0 M AS are calculated directly from the experimental data.

Analyses of potential applied pressure effects on the Form Factor of Ovalbumin

To assess the effects of applied hydrostatic pressure on the ovalbumin form factor, the Kratky plots for the HP-SAXS data were examined, as shown in Figure S6A. For each of the three AS concentrations measured, the Kratky profiles shift down with pressure, as expected due to changes in scattering contrast, but no significant changes to the shape of the profiles are observed. This is consistent with the protein folding resistance to pressure within the range of parameters investigated.

As shown in Figure S6B, the three HP-SAXS series were also analyzed in the range 0.07 Å < Q < 0.2 $Å^{-1}$, where contributions from protein-protein interactions are expected to be weaker and the measured intensities reflect a strong contribution from the form factor. For the various applied hydrostatic pressures measured at 0 M, AS-containing samples, the HP-SAXS data was normalized by the corresponding 10 MPa measurement (where the changes in scattering contrast at different applied pressure were also taken into account). Despite the poorer signal-to-noise of the HP-SAXS data for the 1.2 M and 1.36 M AS-containing solutions, particularly above 0.15 $Å^{-1}$, each of the three normalized data series overlays well, with random oscillations around the average value of 1 as expected in the absence of a significant shift of the form factor.

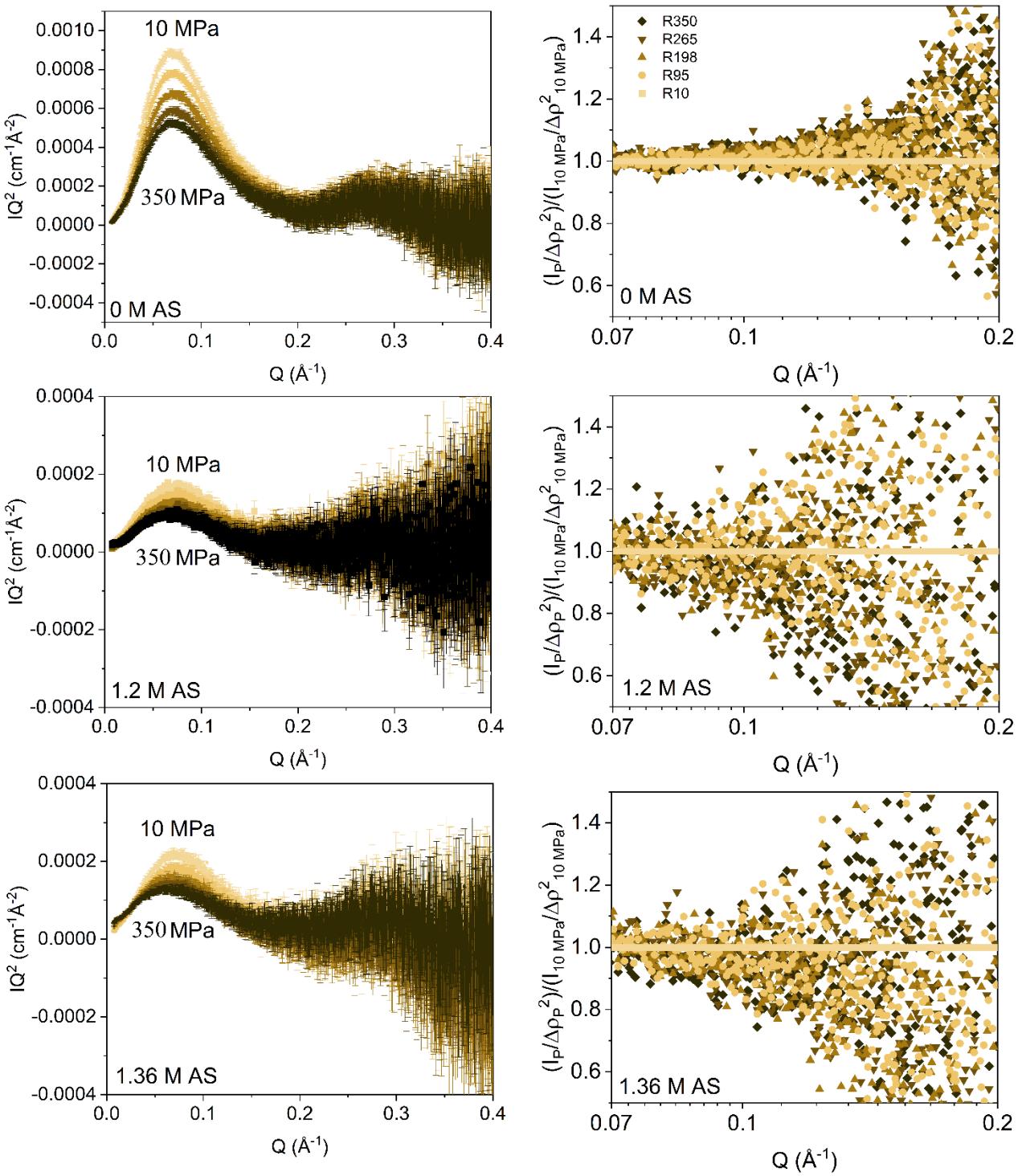

FIGURE S6. (Left) Kratky plots of background-subtracted pressure-series SAXS data, collected at different AS concentrations as labeled for each panel. Applied pressure increases with shade (10 MPa, 98 MPa, 195 MPa, 265 MPa, 350 MPa). Error bars arise from experimental counting statistics. **(Right)** Normalized scattering intensity ratios for the HP-SAXS data sets, calculated for each pressure P from the room pressure data as $R = (I_P/\Delta\rho_P)/(I_{10\ MPa}/\Delta\rho_{10\ MPa})$, where $\Delta\rho$ is the scattering length density contrast for each curve. Applied pressure increases with shade (10 MPa, 98 MPa, 195 MPa, 265 MPa, 350 MPa).

Pitzer osmotic coefficients for common binary electrolytes

$\beta_{MX}^{(0)}$, $\beta_{MX}^{(1)}$, $\beta_{MX}^{(2)}$, and C_{MX}^{ϕ} are empirical parameters, dependent on salt identity as illustrated in Table S5. The error δ is the standard deviation of the residuals for simultaneous of all included parameters.

Table S5. Pitzer parameter values for several common electrolyte pairs [14].

Salt	$z_M : z_X$	$\beta_{MX}^{(0)}\left(\frac{J}{mol}\right)$	$\beta_{MX}^{(1)}\left(\frac{J}{mol}\right)$	$\beta_{MX}^{(2)}\left(\frac{J}{mol}\right)$	$C_{MX}^{\phi}\left(\frac{J}{mol}\right)^2$	Error (δ)
NaCl	1-1	0.077	0.266	0.00	0.001	0.001
NaH_2PO_4	1-1	-0.053	0.040	0.00	0.000	0.003
NH_4Cl	1-1	0.052	0.192	0.00	-0.003	0.001
$NH_4H_2PO_4$	1-1	-0.070	-0.416	0.00	0.007	0.003
$(NH_4)_2SO_4$	1-2	0.041	0.659	0.00	-0.001	0.004
Na_2SO_4	1-2	0.020	1.113	0.00	0.005	0.003
$MgSO_4$	2-2	0.221	3.343	-37.2	0.025	0.004
$AlCl_3$	3-1	0.699	5.845	0.00	0.023	0.005
YCl_3	3-1	0.640	5.444	0.00	-0.023	0.007

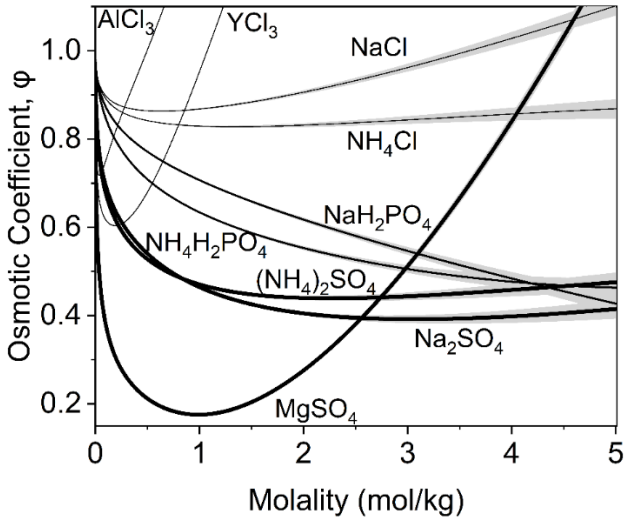

FIGURE S7. Osmotic coefficients at ambient conditions for several common chloride (thin lines), phosphate (normal lines), and sulfate (heavy lines) salts as calculated from the Pitzer correlations. The three anions are common in biological formulations and buffers [15-19]. Error bars, propagated from reported standard deviations in Pitzer empirical parameters, are shown as light gray bands. Rate of departure from non-ideality (decrease from φ=1) and location of φ_{min} depend on ion size and valency.

Comparison of Scattering Intensities for Solutions with Negligible Protein-Protein Interactions

Ovalbumin SAXS measurements at 0.7 M AS on an independent sample set (not included in the master curve calculations) were used to validate the results highlighted in Figure 3a of the main manuscript document, by confirming the AS condition at which b_2^* crosses the zero line. The overlaid intensities in Figure S8 show a good match between the SAXS profiles for dilute (5 mg/ml) ovalbumin without AS, where long-range interactions are assumed to be negligible, and for 15 mg/ml ovalbumin with 0.7 M AS, where $b_2^* = 0$ (Figure 3a).

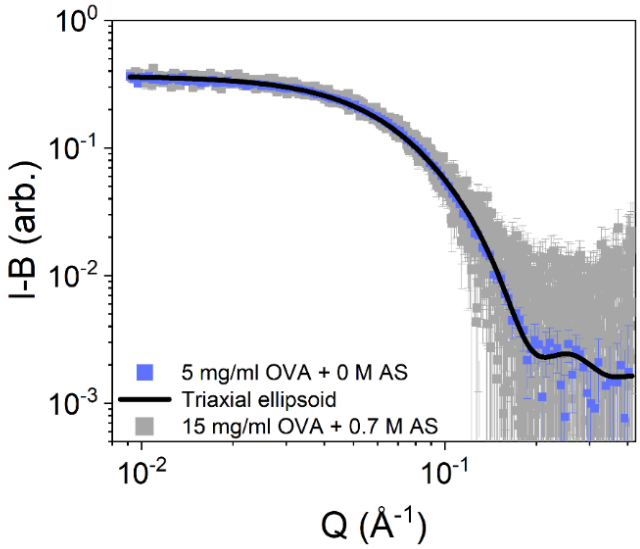

FIGURE S8. Background-subtracted ovalbumin SAXS profiles for 5 mg/ml without the presence of AS (blue) and 15 mg/ml with 0.7 M AS (gray). The profile intensities compare well, validating $b_2^* = 0$ at 0.7 M AS in 15 mg/ml ovalbumin solution as estimated from the master curve. The triaxial ellipsoid form factor fit to the AS-free 5 mg/mL ovalbumin solution also fits the AS-containing 15 mg/mL ovalbumin solution data. Error bars arise from experimental counting statistics.

Calculation of the pressure-dependent density of water

The solvent (water) density was determined from an expression derived from Hooke's law, which related the density of a pure liquid at pressure P to its bulk modulus, K:

$$\rho_P = \frac{\rho_0}{1 - \frac{P - P_0}{K}} \qquad (S5)$$

ρ_0 and ρ_P are the density of water at pressure P_0 and P, respectively. The bulk modulus is itself a function of temperature and pressure. Millero and coworkers investigated properties of both water and deuterium oxide up to 1 kbar (100 MPa), and validated the following equation of state for the bulk modulus as a function of pressure and several temperature-dependent parameters [20, 21]:

$$K = B^* + A_1 P + A_2 P^2 \quad (S6)$$

A_1, A_2, and B^* were determined from fits to experimental data, and are tabulated in the literature for both H_2O and D_2O [20, 21].

Master curve determination

The weighting parameter G was determined by fitting b_2^* as a function of $P_{applied}$ and Π, with a modified stretched exponential as:

$$b_2^* = -\exp\left(\frac{P_{eff}}{P_c}\right)^a + C \quad (S7)$$

where P_c is a characteristic normalization pressure, and a is the critical exponent. $C = b_{2,0}^* + b_{2,s}^*$ where $b_{2,s}^* = 1$ is the contribution from steric repulsion [22] and $b_{2,0}^*$ represents protein interactions beyond steric repulsion at zero effective pressure. It should be noted that equation S7 was used as an empirical numerical approach to parameterize the data; the corresponding parameters are not expected to correlate with a particular physical meaning. The parameters G, a, P_c, and $b_{2,0}^*$ were estimated using the MATLAB Curve Fitter. The goodness of fit was taken as the coefficient of determination $R^2 = 1 - RSS$, where RSS is the sum of the squares of the deviation between experimental and fitted values using a linear regression analysis. $R^2 > 0.7$ was taken as an acceptable fit and $R^2 > 0.9$ as a good fit.

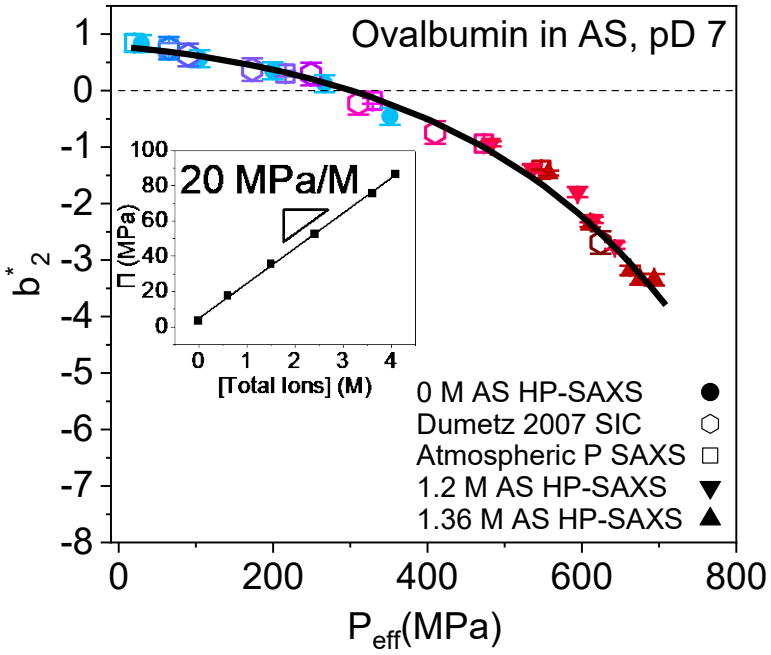

FIGURE S9. Ovalbumin b_2^* master curve (reproduced from Figure 4) with the fit line shown, from the fit parameters in Table S6.

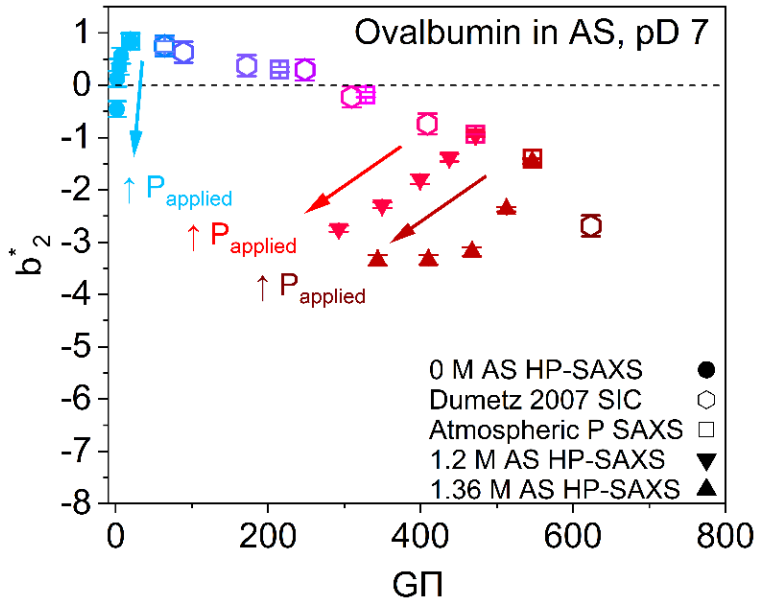

FIGURE S10. Ovalbumin b_2^* as a function of the osmotic pressure contributions, for data collected at various AS concentrations and applied hydrostatic pressures (G = 5.94). Applied hydrostatic pressures for the three HP-SAXS series (blue, 0 M AS; red, 1.2 M AS; dark red, 1.36 M AS) are, in the direction of the arrows: 10, 98, 195, 265, 350 MPa. The hydrostatic pressure for all other points is atmospheric (≈0.1 MPa).

Table S6. Ovalbumin solution conditions for each data point in Figure 4 of the main document. G = 5.94 ± 0.40, P_c = 466 MPa ± 43 MPa, a = 1.29 ± 0.20, and C = 1.77 ± 0.14.

Method	[Protein] (mg/mL)	[AS] (M)	$P_{applied}$ (MPa)	T (°C)	pH	P_{eff} (MPa)	b_2^*
SEC-SAXS	15	0.00	1	22	7.0	20	0.84 ± 0.15
SEC-SAXS	15	0.20	1	22	7.0	64	0.74 ± 0.10
SEC-SAXS	15	0.50	1	22	7.0	214	0.30 ± 0.05
SEC-SAXS	15	0.80	1	22	7.0	326	-0.18 ± 0.05
SEC-SAXS	15	1.20	1	22	7.0	468	-0.94 ± 0.02
SEC-SAXS	15	1.36	1	22	7.0	542	-1.40 ± 0.10
HP-SAXS	15	0.00	10	24	7.0	29	0.83 ± 0.15
HP-SAXS	15	1.20	10	24	7.0	477	-0.94 ± 0.04
HP-SAXS	15	1.36	10	24	7.0	551	-1.46 ± 0.04
HP-SAXS	15	0.00	98	24	7.0	105	0.57 ± 0.15
HP-SAXS	15	1.20	98	24	7.0	531	-1.38 ± 0.09
HP-SAXS	15	1.36	98	24	7.0	606	-2.37 ± 0.04
HP-SAXS	15	0.00	195	24	7.0	200	0.35 ± 0.15
HP-SAXS	15	1.20	195	24	7.0	590	-1.80 ± 0.09
HP-SAXS	15	1.36	195	24	7.0	658	-3.18 ± 0.08
HP-SAXS	15	0.00	265	24	7.0	267	0.12 ± 0.15
HP-SAXS	15	1.20	265	24	7.0	611	-2.29 ± 0.06
HP-SAXS	15	1.36	265	24	7.0	671	-3.34 ± 0.10
HP-SAXS	15	0.00	350	24	7.0	351	-0.46 ± 0.15
HP-SAXS	15	1.20	350	24	7.0	639	-2.74 ± .006
HP-SAXS	15	1.36	350	24	7.0	690	-3.35 ± 0.10
SIC†	5	0.10	1	23	7.0	64	0.75 ± 0.2
SIC†	5	0.25	1	23	7.0	89	0.63 ± 0.2
SIC†	5	0.50	1	23	7.0	171	0.37 ± 0.2
SIC†	5	0.75	1	23	7.0	247	0.29 ± 0.2
SIC†	5	1.00	1	23	7.0	307	-0.22 ± 0.2
SIC†	5	1.25	1	23	7.0	406	-0.74 ± 0.2
SIC†	5	1.50	1	23	7.0	618	-2.69 ± 0.2

All samples were prepared in 5 mM sodium phosphate buffer. †SIC data reproduced from the literature [23]. Error in b_2^* is propagated from error in hydrodynamic radius (0 M AS), estimated from the literature (SIC), or determined from fitting error in Baxter stickiness.

Table S7. β-lactoglobulin (β-LG) solution conditions and composition for each data point in Figure 5a of the main document. G = 8.15 ± 0.87, P_c = 48 MPa ± 7 MPa, a = 0.28 ± 0.10, and C = 3.21 ± 0.64.

Tech.	[β-LG] (mg/mL)	[NaCl] (mM)	$P_{Applied}$ (MPa)	T (°C)	Buffer conditions	P_{eff} (MPa)	b_2^*	Ref
HP-SANS	12	0	0.1	20	†	0.1	3.84 ± 0.15	24
HP-SANS	12	0	20	20	†	20	0.29 ± 0.15	24
HP-SANS	12	0	50	20	†	50	-0.20 ± 0.15	24
HP-SANS	12	0	80	20	†	80	-0.40 ± 0.15	24
HP-SANS	12	0	100	20	†	100	-0.12 ± 0.15	24
HP-SANS	12	0	120	20	†	120	-0.32 ± 0.15	24
HP-SANS	12	0	140	20	†	140	-1.0 ± 0.15	24
Osm.	5-20	5	0	28	‡	2	3.89 ± 0.56	25
Osm.	5-20	10	0	28	‡	5	2.22 ± 0.22	25
Osm.	5-20	15	0	28	‡	7	1.11 ± 0.16	25
Osm.	5-20	50	0	28	‡	27	0.28 ± 0.11	25
Osm.	5-20	100	0	28	‡	60	-0.56 ± 0.28	25
Osm.	5-20	10	0	28	‡	5	1.41 ± 0.38	26
Osm.	5-20	100	0	28	‡	60	0.09 ± 0.56	26
Osm.	2-40	5	0	40	*	2	3.76 ± 0.38	27
Osm.	2-40	25	0	40	*	13	0.71 ± 0.24	27
Osm.	2-40	45	0	40	*	24	-0.09 ± 0.19	27
Osm.	2-40	55	0	40	*	31	-1.41 ± 0.94	27
Osm.	2-40	70	0	40	*	40	-0.19 ± 0.20	27
Osm.	2-40	85	0	40	*	50	-0.28 ± 0.37	27
Osm.	2-40	100	0	40	*	60	-0.47 ± 0.28	27
SLS	10	10	0	25	**	5	2.82 ± 0.19	28
SLS	10	20	0	25	**	10	0.75 ± 0.18	28
SLS	10	25	0	25	**	13	0.56 ± 0.17	28
SLS	10	30	0	25	**	16	0.47 ± 0.19	28
SLS	10	40	0	25	**	21	0.38 ± 0.20	28
SLS	10	50	0	25	**	27	0.19 ± 0.18	28
SLS	10	100	0	25	**	60	0.09 ± 0.28	28
SLS	10	200	0	25	**	131	-0.19 ± 0.30	28
SLS	10	300	0	25	**	209	-0.28 ± 0.27	28

†D_2O, pD 7 ‡H_2O, pH 7 *20 mM MOPS, pH 6.8 **H_2O, pH 6.8. Osm. = Osmometry. Error in b_2^* is estimated from literature data.

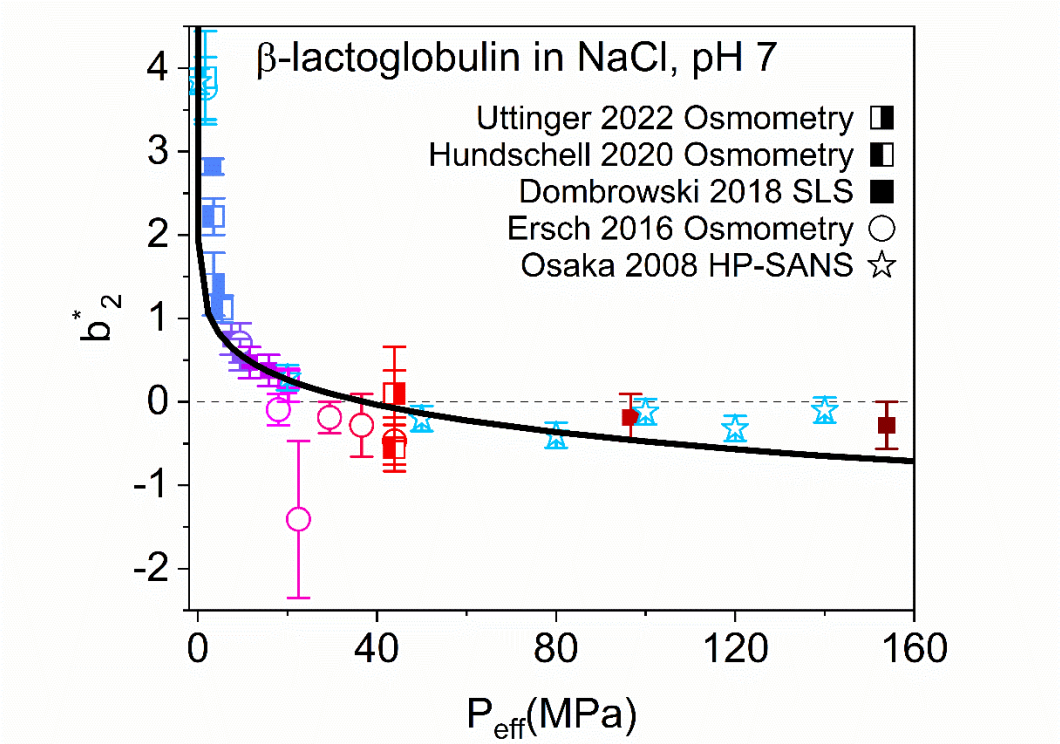

FIGURE S11. β-lactoglobulin (β-LG) b_2^* master curve (reproduced from Figure 5a) with the fit line shown, from the fit parameters in Table S6.

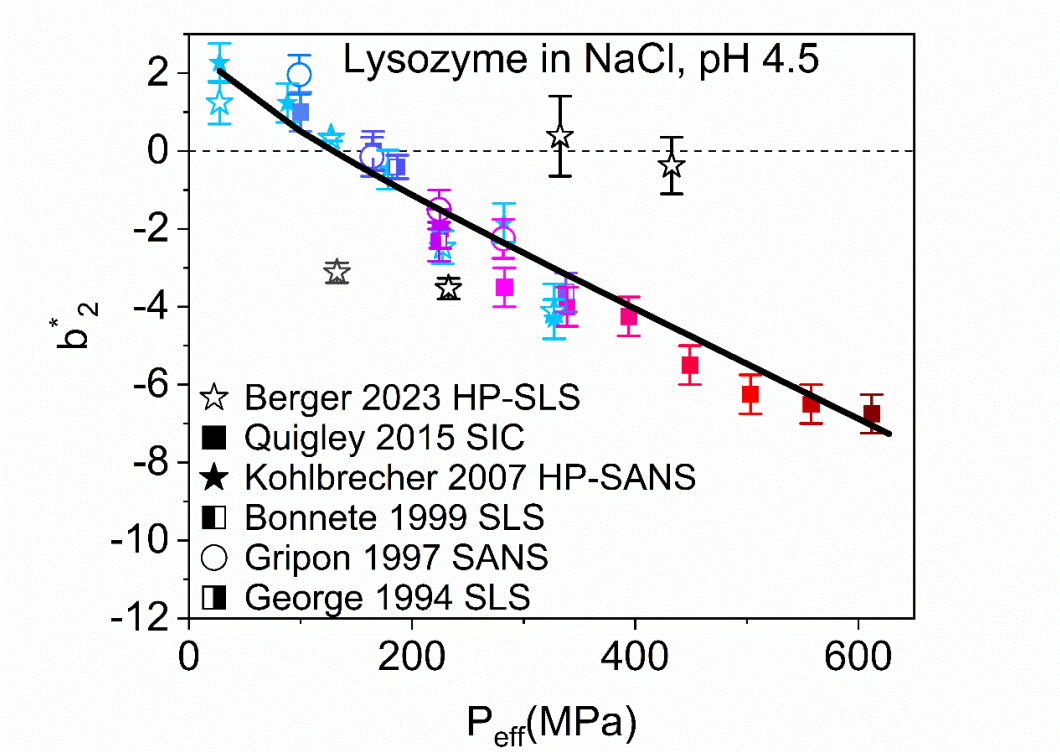

FIGURE S12. Lysozyme b_2^* master curve (reproduced from Figure 5b) with the fit line shown, from the fit parameters in Table S6.

Table S8. Lysozyme (LYS) solution conditions and composition for each data point in Figure 5b of the main document. G = 5.22 ± 0.53, P_c = 235 MPa ± 26 MPa, a = 0.89 ± 0.11, and C = 1.84 ± 0.21.

Technique	[LYS] (mg/mL)	[NaCl] (M)	$P_{Applied}$ (MPa)	T (°C)	Buffer	P_{eff} (MPa)	b_2^*	Ref
HP-SLS	1-10	0.00	0.1	20	50 mM, pH 4.6	24	1.24 ± 0.55	[29]
HP-SLS	1-10	0.00	100	20	50 mM, pH 4.6	124	0.34 ± 0.08	[29]
HP-SLS	1-10	0.00	200	20	50 mM, pH 4.6	224	-2.47 ± 0.43	[29]
HP-SLS	1-10	0.00	300	20	50 mM, pH 4.6	324	-4.12 ± 0.71	[29]
HP-SLS	1-10	0.15	0.1	20	50 mM, pH 4.6	115	-3.13 ± 0.26	[29]
HP-SLS	1-10	0.15	100	20	50 mM, pH 4.6	215	-3.54 ± 0.27	[29]
HP-SLS	1-10	0.15	200	20	50 mM, pH 4.6	315	0.38 ± 1.03	[29]
HP-SLS	1-10	0.15	300	20	50 mM, pH 4.6	415	-0.37 ± 0.73	[29]
SIC	15	0.10	1	25	20 mM, pH 4.5	87	1.00 ± 0.48	[18]
SIC	15	0.20	1	25	20 mM, pH 4.5	144	0.00 ± 0.48	[18]
SIC	15	0.30	1	25	20 mM, pH 4.5	196	-2.00 ± 0.48	[18]
SIC	15	0.40	1	25	20 mM, pH 4.5	246	-3.50 ± 0.48	[18]
SIC	15	0.50	1	25	20 mM, pH 4.5	295	-4.00 ± 0.48	[18]
SIC	15	0.60	1	25	20 mM, pH 4.5	343	-4.25 ± 0.48	[18]
SIC	15	0.70	1	25	20 mM, pH 4.5	391	-5.50 ± 0.48	[18]
SIC	15	0.80	1	25	20 mM, pH 4.5	438	-6.25 ± 0.48	[18]
SIC	15	0.90	1	25	20 mM, pH 4.5	485	-6.50 ± 0.48	[18]
SIC	15	1.00	1	25	20 mM, pH 4.5	532	-6.75 ± 0.48	[18]
SLS	1-25	0.30	0	25	50 mM, pH 4.5	195	-2.33 ± 0.42	[30]
SLS	1-25	0.50	0	25	50 mM, pH 4.5	294	-3.63 ± 0.42	[30]
SLS	20	0.25	0	25	40 mM, pH 4.3	163	-0.41 ± 0.30	[31]
SANS	50	0.10	0	25	50 mM, pH 4.5	86	1.96 ± 0.51	[32]
SANS	50	0.20	0	25	50 mM, pH 4.5	143	-0.15 ± 0.51	[32]
SANS	50	0.30	0	25	50 mM, pH 4.5	195	-1.50 ± 0.51	[32]
SANS	50	0.40	0	25	50 mM, pH 4.5	245	-2.26 ± 0.51	[32]

All samples were prepared in sodium acetate buffer. Error in b_2^* is estimated from literature data.

DISCLAIMER

Certain instruments and software are identified to foster understanding. Such identification does not imply recommendation or endorsement by the National Institute of Standards and Technology, nor does it imply that the instruments and software identified are necessarily the best available for the purpose. The statements, findings, conclusions and recommendations are those of the authors and do not necessarily reflect the view

of NIST, the National Institute of General Medical Sciences, the National Institutes of Health. or the U.S. Department of Commerce.

REFERENCES

(1) Brookes, E.; Vachette, P.; Rocco, M.; Pérez, J. US-SOMO HPLC-SAXS module: dealing with capillary fouling and extraction of pure component patterns from poorly resolved SEC-SAXS data. *J. Appl. Crystallogr.* **2016**, *49* (5), 1827-1841. DOI: 10.1107/s1600576716011201.
(2) Hopkins, J.; Gillilan, R.; Skou, S. BioXTAS RAW 2.0: the latest in SAXS data analysis. *Acta Crystallogr., Sect. A: Found. Adv.* **2020**, *76* (a1), a27-a27. DOI: 10.1107/s0108767320099729.
(3) Alexander, M.; Dalgleish, D. G. Dynamic Light Scattering Techniques and Their Applications in Food Science. *Food Biophys.* **2006**, *1* (1), 2-13. DOI: 10.1007/s11483-005-9000-1.
(4) Roosen-Runge, F.; Gulotta, A.; Bucciarelli, S.; Casal-Dujat, L.; Garting, T.; Skar-Gislinge, N.; Obiols-Rabasa, M.; Farago, B.; Zaccarelli, E.; Schurtenberger, P.; Stradner, A. Crowding in the eye lens: Modeling the multisubunit protein beta-crystallin with a colloidal approach. *Biophys. J.* **2020**, *119* (12), 2483-2496. DOI: 10.1016/j.bpj.2020.10.035.
(5) Miles, A. J.; Ramalli, S. G.; Wallace, B. A. DichroWeb, a website for calculating protein secondary structure from circular dichroism spectroscopic data. *Protein Sci.* **2022**, *31* (1), 37-46. DOI: 10.1002/pro.4153.
(6) Lees, J. G.; Miles, A. J.; Wien, F.; Wallace, B. A. A reference database for circular dichroism spectroscopy covering fold and secondary structure space. *Bioinformatics* **2006**, *22* (16), 1955-1962. DOI: 10.1093/bioinformatics/btl327.
(7) Provencher, S. W.; Gloeckner, J. Estimation of globular protein secondary structure from circular dichroism. *Biochemistry* **1981**, *20* (1), 33-37. DOI: 10.1021/bi00504a006.
(8) Moré, J. J. The Levenberg-Marquardt algorithm: Implementation and theory. *Numer. Anal.* **1978**, 105-116. DOI: 10.1007/bfb0067700.
(9) Feigin, L. S., Dmitri. *Struct. Anal. Small-Angle X-Ray Neutron Scattering*; Spring Science, 1987.
(10) Schneidman-Duhovny, D.; Hammel, M.; Tainer, J. A.; Sali, A. FoXS, FoXSDock and MultiFoXS: Single-state and multi-state structural modeling of proteins and their complexes based on SAXS profiles. *Nucleic Acids Res.* **2016**, *44* (W1), W424-429. DOI: 10.1093/nar/gkw389.
(11) Svergun, D. I. Determination of the Regularization Parameter in Indirect-Transform Methods Using Perceptual Criteria. *J. Appl. Crystallogr.* **1992**, *25* (4), 495-503. DOI: Doi 10.1107/S0021889892001663.
(12) Parmar, A. S.; Muschol, M. Hydration and hydrodynamic interactions of lysozyme: effects of chaotropic versus kosmotropic ions. *Biophys. J.* **2009**, *97* (2), 590-598. DOI: 10.1016/j.bpj.2009.04.045.
(13) Kristiansen, K. R.; Otte, J.; Ipsen, R.; Qvist, K. B. Large-scale Preparation of β-Lactoglobulin A and B by Ultrafiltration and Ion-exchange Chromatography. *Int. Dairy J.* **1998**, *8*, 113-118.
(14) Pitzer, K. S. *Activity coefficients in electrolyte solutions*; CRC Press, 1991.
(15) Beck, C.; Grimaldo, M.; Braun, M. K.; Bühl, L.; Matsarskaia, O.; Jalarvo, N. H.; Zhang, F.; Roosen-Runge, F.; Schreiber, F.; Seydel, T. Temperature and salt controlled tuning of protein clusters. *Soft Matter* **2021**, *17* (37), 8506-8516. DOI: 10.1039/d1sm00418b.
(16) Greene, D. G.; Modla, S.; Wagner, N. J.; Sandler, S. I.; Lenhoff, A. M. Local Crystalline Structure in an Amorphous Protein Dense Phase. *Biophys. J.* **2015**, *109*, 1716-1723.

(17) Cardinaux, F. D. R.; Zaccarelli, E.; Stradner, A.; Bucciarelli, S.; Farago, B.; Egelhaaf, S. U.; Sciortino, F.; Schurtenberger, P. Cluster-Driven Dynamical Arrest in Concentrated Lysozyme Solutions. *J. Phys. Chem. B* **2011**, *115* (22), 7227-7237. DOI: 10.1021/jp112180p.
(18) Quigley, A.; Williams, D. R. The second virial coefficient as a predictor of protein aggregation propensity: A self-interaction chromatography study. *Eur. J. Pharm. Biopharm.* **2015**, *96*, 282-290. DOI: 10.1016/j.ejpb.2015.07.025.
(19) Wang, G.; Wang, S.; Wu, H.; Yan, C.; Liu, Y. Interactions of Bovine Serum Albumin Molecules in an Aqueous Sodium Sulfate Solution Determined by an Osmotic Pressure Method. *J. Solution Chem.* **2018**, *47* (3), 586-594. DOI: 10.1007/s10953-018-0738-8.
(20) Millero, F. J.; Fine, R. A. Compressibility of water as a function of temperature and pressure. *J. Chem. Phys.* **1973**, *59*, 5529-5536.
(21) Millero, F. J.; Fine, R. A. The high pressure PVT properties of deuterium oxide. *J. Chem. Phys.* **1975**, *63*, 89-95.
(22) Blanco, M. A.; Perevozchikova, T.; Martorana, V.; Manno, M.; Roberts, C. J. Protein-protein interactions in dilute to concentrated solutions: alpha-chymotrypsinogen in acidic conditions. *J. Phys. Chem. B* **2014**, *118* (22), 5817-5831. DOI: 10.1021/jp412301h.
(23) Dumetz, A. C.; Snellinger-O'brien A, M.; Kaler, E. W.; Lenhoff, A. M. Patterns of protein protein interactions in salt solutions and implications for protein crystallization. *Protein Sci.* **2007**, *16* (9), 1867-1877. DOI: 10.1110/ps.072957907.
(24) Osaka, N.; Takata, S.-i.; Suzuki, T.; Endo, H.; Shibayama, M. Comparison of heat- and pressure-induced gelation of β-lactoglobulin aqueous solutions studied by small-angle neutron and dynamic light scattering. *Polymer* **2008**, *49* (12), 2957-2963. DOI: 10.1016/j.polymer.2008.04.055.
(25) Hundschell, C. S.; Bäther, S.; Drusch, S.; Wagemans, A. M. Osmometric and viscometric study of levan, β-lactoglobulin and their mixtures. *Food Hydrocolloids* **2020**, *101*, 105580. DOI: 10.1016/j.foodhyd.2019.105580.
(26) Uttinger, M. J.; Hundschell, C. S.; Lautenbach, V.; Pusara, S.; Bäther, S.; Heyn, T. R.; Keppler, J. K.; Wenzel, W.; Walter, J.; Kozlowska, M.; Wagemans, A. M.; Peukert, W. Determination of specific and non-specific protein–protein interactions for beta-lactoglobulin by analytical ultracentrifugation and membrane osmometry experiments. *Soft Matter* **2022**, *18* (35), 6739-6756. DOI: 10.1039/d2sm00908k.
(27) Ersch, C.; Meijvogel, L. L. C.; van der Linden, E.; Martin, A.; Venema, P. Interactions in protein mixtures. Part I: Second virial coefficients from osmometry. *Food Hydrocolloids* **2016**, *52*, 982-990. DOI: 10.1016/j.foodhyd.2015.07.020.
(28) Dombrowski, J.; Gschwendtner, M.; Saalfeld, D.; Kulozik, U. Salt-dependent interaction behavior of β-Lactoglobulin molecules in relation to their surface and foaming properties. *Colloids Surf., A* **2018**, *558*, 455-462. DOI: 10.1016/j.colsurfa.2018.09.015.
(29) Berger, J. E.; Teixeira, S. C. M.; Sloey, C. J.; Qi, W.; Roberts, C. J. High Pressure Light Scattering of Therapeutic Proteins To Probe Aggregation and Protein-Protein Interactions. *J. Phys. Chem. B* **2023**, *127* (26), 5742-5754. DOI: 10.1021/acs.jpcb.2c09118.
(30) Bonnete, F.; Finet, S.; Tardieu, A. Second virial coefficient: variations with lysozyme crystallization conditions. *J. Cryst. Growth* **1999**, *196*, 403-414.
(31) George, A.; Wilson, W. W. Predicting protein crystallization from a dilute solution property. *Acta Crystallogr., Sect. D. Biol. Crystallogr.* **1994**, *50* (4), 361-365. DOI: 10.1107/s0907444994001216.
(32) Kohlbrecher, J.; Bollhalder, A.; Vavrin, R.; Meier, G. A high pressure cell for small angle neutron scattering up to 500 MPa in combination with light scattering to investigate liquid samples. *Rev. Sci. Instrum.* **2007**, *78* (12), 125101. DOI: 10.1063/1.2817632.